Published online 19 May 2017

Nucleic Acids Research, 2017, Vol. 45, No. 12 ***7031–7041***
doi: 10.1093/nar/gkx427

Modulation of cyclobutane thymine photodimer formation in T_{11}-tracts in rotationally phased nucleosome core particles and DNA minicircles

Kesai Wang and John-Stephen A. Taylor*

Department of Chemistry, Washington University, St Louis, MO 63130, USA

Received February 03, 2017; Revised May 01, 2017; Editorial Decision May 02, 2017; Accepted May 11, 2017

ABSTRACT

Cyclobutane pyrimidine dimers (CPDs) are DNA photoproducts linked to skin cancer, whose mutagenicity depends in part on their frequency of formation and deamination. Nucleosomes modulate CPD formation, favoring outside facing sites and disfavoring inward facing sites. A similar pattern of CPD formation in protein-free DNA loops suggests that DNA bending causes the modulation in nucleosomes. To systematically study the cause and effect of nucleosome structure on CPD formation and deamination, we have developed a circular permutation synthesis strategy for positioning a target sequence at different superhelix locations (SHLs) across a nucleosome in which the DNA has been rotationally phased with respect to the histone octamer by TG motifs. We have used this system to show that the nucleosome dramatically modulates CPD formation in a T_{11}-tract that covers one full turn of the nucleosome helix at seven different SHLs, and that the position of maximum CPD formation at all locations is shifted to the 5′-side of that found in mixed-sequence nucleosomes. We also show that an 80-mer minicircle DNA using the same TG-motifs faithfully reproduces the CPD pattern in the nucleosome, indicating that it is a good model for protein-free rotationally phased bent DNA of the same curvature as in a nucleosome, and that bending is modulating CPD formation.

INTRODUCTION

It is well established that DNA photoproducts produced by sunlight are responsible for the majority of the mutations associated with skin cancers (1–4). What is not so well established is the physical or mechanistic origin of the variation in mutation type and frequency within a gene, which must result from a complex interplay between the frequency of photoproduct formation, chemical transformation, repair and translesion synthesis. To begin to dissect the various contributions of these factors, we have been examining the role of chromatin structure on DNA photoproduct formation and subsequent deamination. It was demonstrated many decades ago that nucleosomes can modulate cyclobutane pyrimidine dimer (CPD) formation in mixed sequence genomic DNA with a 10–11 bp periodicity that was attributed to the effect of bending on the conformation and dynamics of DNA (5,6). A similar effect was observed to occur in a protein-free DNA loop which supported the idea that bending, and not protein DNA interactions were the primary cause of the modulation of photoproduct formation (7).

The original studies of CPD modulation by nucleosomes were carried out with nucleosomes containing mixed sequence DNA obtained from the degradation of chromatin. Such sequences may be biased to bend around the nucleosome and obscure the relationship between sequence, rotational position and CPD formation. In a study of 254 nm induced CPD formation in nucleosome bound 5S rRNA gene with a defined sequence, a <2-fold modulation of CPD formation could be detected only after carefully subtracting the CPD pattern produced in free DNA (8). In contrast, HISAT DNA from the yeast DED1 promoter containing various length T-tracts showed strong modulation of CPD formation, but with maxima that were shifted to the 5′-side of what was observed with mixed sequence nucleosomal DNA (9). A more recent study measuring rates of CPD formation and photostationary state levels induced by 254 nm light concluded that there was no modulation of photoproduct formation in 5S and Widom 601 defined sequence DNAs (10). In contrast, UVB-induced CPD formation of TCG CPDs at every rotational position in a full turn of DNA at the dyad axis of a rotationally phased artificial DNA sequence was modulated in a similar way to what was observed with mixed sequence DNA. We also discovered that the deamination of C and 5-methylcytosine (^{m}C) in the CPDs was modulated with the same rotational phasing as their formation (11). Because deamination of C and ^{m}C in CPDs has been correlated with C to T signature mutations induced by UV light (3,12), it would be of interest

*To whom correspondence should be addressed. Tel. +1 314 935 6721; Fax: +1 314 935 4481; Email: taylor@wustl.edu

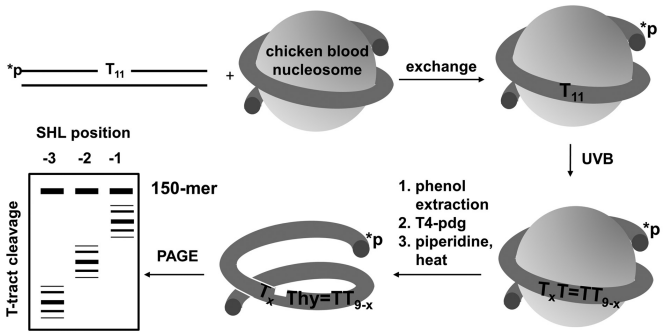

Figure 1. Strategy for studying CPD formation as a function of rotational and translational position in a nucleosome. A 150-mer, 5′-^{32}P-endlabeled duplex DNA containing a T_{11}-tract at various translational positions is incorporated into a nucleosome by a salt-mediated exchange mechanism and then irradiated with UVB light. The DNA is then treated with T4-pdg which cleaves the DNA at sites of CPDs, and electrophoresed on a denaturing polyacrylamide gel to visualize the sites of cleavage.

to know whether the deamination is also being modulated by bending or by some other effect.

To investigate the modulation of CPD formation and deamination by nucleosomes, and in bent DNA, we have first chosen to develop methodology to study CPD formation at different translational positions (superhelix locations, SHLs) in a nucleosome (Figure 1) and in a DNA minicircle. A T_{11}-tract was chosen as a model system for study because it contains all 10 possible CPD sites in a full turn of DNA. To hold the T_{11}-tract in a single rotational orientation in a nucleosome, and in minicircle DNA, we have made use of TG bending motifs $(T/A)_3NN(G/C)_3NN$ (Figure 2A) discovered by Crothers *et al.* to rotationally fix nucleosomal DNA when spaced every 10 bp (13). To position the T_{11}-tract at different SHLs in a nucleosome, we made use of a circular permutation synthesis strategy (Figure 2B) of the type initially developed by Crothers for localizing bends (14). We will show that CPD formation in the T_{11}-tracts is strongly modulated by a nucleosome, with maxima that are shifted to the 5′-side in the T_{11}-tract containing strand compared to mixed sequence DNA as previously observed for a mixture of various length T-tracts (9). The precise position of the maxima, however, varied with the translational position and did not correlate exactly with the maxima of hydroxyl radical (HO·) cleavage sites used to assign rotational orientation of the DNA. To study CPD formation in protein-free DNA with the same curvature as in the nucleosome, we prepared a rotationally phased 80-mer minicircle DNA. CPD formation in the minicircle DNA was also found to be modulated in the same way as in the nucleosome, indicating that the TG motifs were rotationally phasing the minicircles and that bending was the major factor in controlling CPD formation frequency.

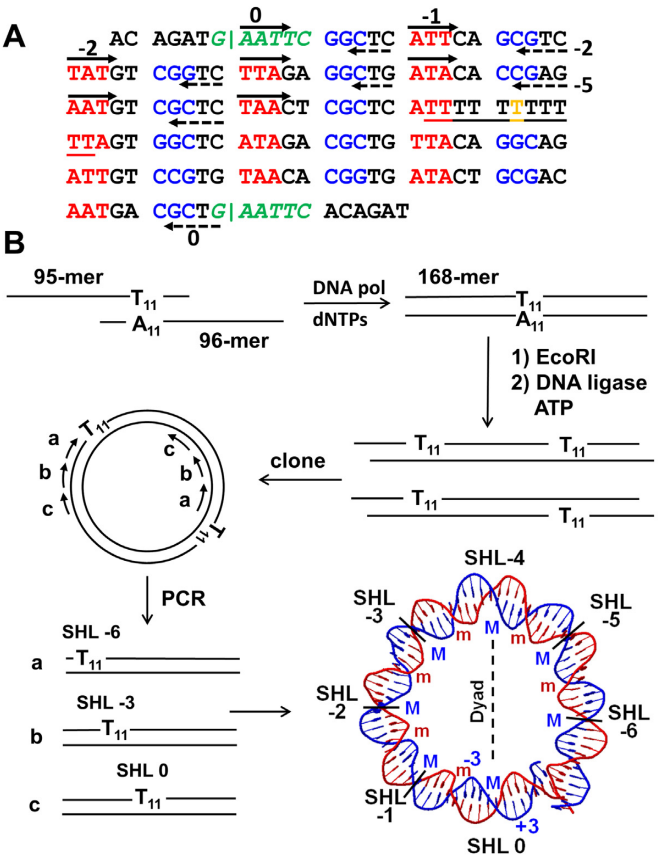

Figure 2. Circular permutation polymerase chain reaction (PCR) strategy used for preparing nucleosomal DNA with T_{11}-tracts at specific superhelix locations (SHLs). (**A**) A 168-mer DNA duplex was designed to have a centrally located T_{11}-tract (underlined), terminal EcoRI restriction sites (green italic), phased minor groove bending $(T/A)_3$ sequences in red and major groove bending $(G/C)_3$ sequences in blue. The T in orange in the T_{11}-tract corresponds to the position at which the major groove is expected to bend toward the histone surface at the dyad axis. (**B**) The 168-mer DNA duplex was prepared by primer extension of two overlapping 95 and 96-mers, cleaved with EcoRI and multimerized with T4 DNA ligase and adenosine triphosphate. The dimer was then excised from a gel and cloned. Nucleosomal DNAs with T_{11}-tracts at specific SHLs were prepared from the clone by PCR using specific pairs of forward and reverse primers (Supplementary Figure S3) whose positions are shown as solid and dashed arrows respectively on the sequence in panel A. The SHLs are identified by the number of helical turns from the dyad axis on the blue strand containing the T_{11}-tract. They are negative to correspond with the negative numbers assigned to nucleotides on the T_{11}-tract strand that are 5′-to the T at the dyad axis which is assigned as 0. The −3 (inside) and +3 (outside) nucleotide positions are shown in blue. The positions at which the major and minor grooves face the histone surface are indicated by M and m, respectively, and are colored coded blue and red to match the major groove and minor groove bending motifs in panel A.

MATERIALS AND METHODS

Materials

Oligodeoxynucleotides (ODNs) were from Integrated DNA technologies (IDT). T4-pdg (pyrimidine dimer glycosylase, previously known as T4 endonuclease V) was prepared from a clone provided from Stephen Llyod as previously described (15).

Nucleosomal DNA dimers

The 168-bp parental nucleosomal DNA duplex was synthesized by hybridization of 95-mer and 96-mer ODNs (IDT) to form a 23-bp duplex at their 3′-ends by slowly cooling from 95°C to room temperature in 50 mM NaCl, and extended by 3′ to 5′-exo$^-$ Klenow Fragment (New England Bi-

oLabs) in 50 mM NaCl, 10 mM Tris–HCl (pH 7.5), 10 mM $MgCl_2$, 100 μM dNTPs and 1 mM dithiothreitol (DTT), for 30 min at 37°C. The 168-bp duplex DNA was then digested by EcoRI (Promega) in 90 mM Tris–HCl (pH 7.5), 50 mM NaCl and 10 mM $MgCl_2$, for 30 min at 37°C, and oligomerized with T4 DNA ligase (Promega) in 30 mM Tris–HCl (pH 7.8), 10 mM $MgCl_2$, 10 mM DTT and 1 mM adenosine triphosphate (ATP), for 3 h at room temperature. The dimer product was separated by electrophoresis on a 3% agarose gel run at 200 V and isolated using a Promega Wizard SV gel and polymerase chain reaction (PCR) clean-up system. The dimeric DNA was then cloned into pBlueScript II SK- vector DNA (Agilent) that had been restricted with EcoRI and then dephosphorylated with calf intestinal phosphatase (CIP) (New England Biolabs) in 100 mM NaCl, 50 mM Tris–HCl (pH 7.5), 10 mM $MgCl_2$ and 1 mM DTT, for 30 min, at 37°C, to prevent re-circularization. The cloning was performed using 1:1, 1:3 and 3:1 molar ratios of vector:insert with T4 DNA ligase and 1 mM ATP at 10°C overnight. The pBS vector with the dimer insert was then transfected into TOP10 chemically competent *Escherichia coli* cells (from Invitrogen) and plated on solid LB media (15 g/l agar, 25 g/l LB broth, 100 μg/ml ampicillin). A clone containing the desired dimer plasmid was identified by restriction analysis and the sequence verified by DNA sequencing.

Circular permutation synthesis of nucleosomal DNA

The pBS dimer-containing clone was cultured in liquid LB media (25 g/l LB broth and 100 μg/ml ampicillin) and the plasmid was harvested with Promega PureYield plasmid miniprep system. Translationally permuted 150-bp nucleosomal DNAs were prepared from this plasmid by PCR amplification with LongAmp Taq DNA polymerase (New England Biolabs) for 35 cycles followed by phenol extraction and ethanol precipitation. A typical 100 μl PCR reaction contained 0.5 μM of forward and reverse primers, 300 μM of dNTPs, 300 ng template DNA, 4 μl DNA polymerase in 60 mM Tris-SO_4 (pH 9.0), 20 mM $(NH_4)_2SO_4$, 2 mM $MgSO_4$, 3% glycerol, 0.06% IGEPAL CA-630 and 0.05% Tween 20.

Nucleosome reconstitution

Nucleosome core particles (NCPs) were isolated and purified from chicken erythrocytes following a simplified procedure provided by Dr. Michael Smerdon. DNA duplex 150-mers corresponding to seven different translational positions were incorporated into the nucleosomes by a salt mediated exchange process. Briefly, 150-bp duplex was incubated with nucleosomes at various ratios in 300 μl of 2 M NaCl, 10 mM Tris–HCl, 5 mM ethylenediaminetetraacetic acid (EDTA) at pH 7.5 and room temperature for 2 h, and then dialyzed against 50 mM NaCl, 10 mM Tris–HCl, pH 7.5, at 4°C, overnight. The reconstituted nucleosomal core particles were recovered from the dialysis tubing and equilibrated at 54°C for 2 h to fix the nucleosomal phasing. The reconstituted particles were assayed by native polyacrylamide gel electrophoresis (PAGE) (6% acylamide, 0.2% bisacrylamide in 100 mM Tris-Borate 2 mM EDTA (TBE) and the ratio of nucleosome-bound DNA to free DNA was quantified by Quantity One software.

Relative binding affinity of circularly permuted sequences

The relative binding affinities for the nucleosomal DNAs for the histone core particle were determined by a competitive nucleosome reconstitution experiment with chicken DNA that was purified from isolated nucleosomes by phenol extraction and ethanol precipitation by a general procedures (13,16). In a first step, a fixed amount of radiolabeled nucleosomal SHL 0 DNA was incubated with chicken blood NCPs (1:550) and increasing amounts of competitor chicken nucleosomal DNA at 2 M NaCl, after which the salt concentration was lowered to 50 mM, and the reaction mixtures electrophoresed on a native polyacrylamide gel (6% acylamide, 0.2% bisacrylamide in TBE). In this way it was determined that 385 parts of chicken DNA was needed to give ∼50% binding of the radiolabeled nucleosomal SHL 0 DNA. Then radiolabeled SHL 0 to −6 DNAs were incubated in triplicate with the competitor DNA and NCPs in a 1:385:550 ratio, and the average ratios of bound to free DNA were calculated relative to that for the SHL 0 DNA.

Circular 80-mer DNA substrates

The single strand circular 80-mer DNA containing an A_{11}-tract was prepared by ligation of the linear DNA with T4 DNA ligase and 1 mM ATP in the presence of a scaffold DNA at 10°C overnight and purified by denaturing PAGE on a 10% acrylamide 0.33% bisacrylamide gel in 7 M urea in TBE. Purified ligation products were then treated with 5 μl of exonuclease I (New England Biolabs) in 67 mM glycine-KOH, 6.7 mM $MgCl_2$, 10 mM 2-mercaptoethanol, pH 9.5 for 1 h at 37°C to eliminate any unligated, and ligated, single-stranded, linear DNAs. The circular DNA was then annealed with complementary single strand T_{11}-tract containing ODNs of different lengths in 50 mM NaCl by slowly cooling from 90°C to room temperature. Annealed products were purified by native PAGE on 6% acrylamide, 0.2% bisacrylamide gel in TBE before further treatment.

Hydroxyl radical footprinting

Sodium ascorbate, $Fe(NH_4)_2$ $(SO_4)_2{\cdot}6H_2O$ and H_2O_2 (15 mM, 1.5 mM and 0.18% final concentrations respectively) were quickly added to 100 μl of the nucleosome-bound DNA sample in 50 mM NaCl, 10 mM Tris–HCl, pH 7.5 reaction buffer with gentle vortexing after the addition of each reagent. The reaction was incubated for 120 s at room temperature and quenched by addition of glycerol and EDTA solution to final concentrations of 5% and 12 mM, respectively. The samples were electrophoresed on a native PAGE (6% acylamide, 0.2% bisacrylamide in TBE), and gel sections containing the nucleosome bands were excised, crushed and soaked in 1% sodium dodecyl sulphate and 0.2 M NaCl. The proteins were then extracted with phenol:chloroform:isopropanol 25:24:1, and the DNA was ethanol precipitated. To align the bands, a Maxam-Gilbert G sequencing reaction was carried out on the nucleosome-free DNA sample in 50 mM cacodylate, 50 mM NaCl,

5 mM EDTA at pH 8.2. For a 100 μl reaction, 1 μl of dimethyl sulfate was added to initiate the reaction. After 120 s of incubation at room temperature, 60 μl of mercaptoethanol was added to quench the reaction. The DNA was ethanol-precipitated and the resulting pellet was solubilized in 100 μl of 1 M piperidine, followed by 5 min heating at 90°C and evaporating to dryness at 60°C.

T4-pdg Assay for CPDs

DNA substrates were irradiated with broad band UVB light (280–400 nm, centered at 312 nm) (Spectroline model XX-15B) at 0 and 40°C at a measured intensity of 1.5 mW/cm^2 for 40 min for a dose of 36 kJ/m^2. Nucleosome-bound DNA was first extracted with phenol:chloroform:isopropanol 25:24:1 twice, and ethanol-precipitated twice. The DNA samples were incubated with 8 μg of T4-pdg in 10 mM Tris–HCl, 50 mM NaCl, 5 mM EDTA, pH 7.5 for 30 min at 37°C and then heated at 90°C in 1M piperidine for 5 min to insure complete elimination of the sugar ring. Residual piperidine was evaporated by heating at 60°C *in vacuo*. The resulting pellets were brought up in 20 μl formamide-dye and sequentially loaded on a 10% denaturing PAGE (7M urea, 10% acrylamide, 0.33% bisacrylamide in 1 × TBE) so that the T-tracts would be aligned.

Peak analysis

The volume tool in Quantity One was used to quantitatively determine the relative amounts of HO· cleavage and TT CPD formation as a function of nucleotide position x, and the relative peak volumes I were fit to a Gaussian function, $I = C + a*\exp(-(x-b)^2/(2*c^2))$ where C is a constant, a is the amplitude, b is the position of the maximum and c is the standard deviation.

Relative photoreactivity of T_{11}-tracts at different SHLs

To determine the relative efficiency of CPD formation in different SHLs, the 5′-radiolabeled duplex 41-mer sequence was separately mixed with 5′-radiolabeled duplex SHL -1 and -2 nucleosomal DNA. The mixtures were electrophoresed to determine the exact ratio of the 41-mer to the nucleosomal DNA by volume integration of the bands in a radioimage of the gel. The mixtures were then exchanged with the chicken NCPs, irradiated and then subjected to the T4-pdg assay described above to determine the relative photoreactivity of the T-tracts at the SHL −1 and −2 positions in the NCP DNA relative to that of the unbound 41-mer DNA. Two separate mixtures of 5′-radiolabeled duplex DNA, one consisting of SHL 0, −2, −4 and −6 DNA, and the other of SHL −1, −3 and −5 DNA were then prepared, a fraction of each which was assembled into an NCP. The free and NCP DNAs were then irradiated and subjected to the T4 endonuclease assay from which the relative reactivities of the T-tracts at the different SHLs were calculated.

RESULTS AND DISCUSSION

Design and synthesis of the DNA substrates

To facilitate the synthesis of nucleosomal DNA containing a T_{11}-tract at each of the seven SHLs in the 5′-half of an NCP, we adopted a circular permutation synthesis strategy (Figure 2) of the type originally developed by Crothers *et al.* to study DNA bending (14). The idea was to synthesize a single nucleosomal DNA sequence containing a T_{11}-tract and then to dimerize it, after which nucleosomal DNA containing the T_{11}-tract in any desired SHL could be obtained by PCR using the appropriate primers (Figure 2B and Supplementary Figure S3). The parental nucleosomal DNA was designed to have the T_{11}-tract centered at the dyad axis by incorporating TG bending motifs, $(T/A)_3NN(G/C)_3NN$, every 10 bp in the flanking DNA (Figure 2A) (13,17). With this bending motif, bending is toward the major groove at the central GC base pair of the $(G/C)_3$ sequence and toward the minor groove at the central TA base pair of the $(T/A)_3$ sequence (Figure 2B). In this way, the central T of the T_{11}-tract in the parent 150-mer maps to 0, the dyad axis, and the T's to the 5′-side are assigned negative numbers, and to the 3′-side, positive numbers. To make dimers of the nucleosomal DNA, EcoRI digestion sites were engineered into the ends of the sequence without interrupting the TG motifs, and were flanked by an extra 6 bp to ensure efficient digestion. The resulting 168-mer sequence was also designed not to contain repetitive sequences as previously used (13,17) to insure that unique primers could be used to amplify any desired nucleosomal DNA sequence.

The designed 168-mer DNA was prepared by primer extension of two overlapping 95-mer and 96-mer synthetic ODNs. The dimer of the 150-mer nucleosomal DNA was prepared by digesting the 168-mer with EcoRI and ligating the digestion products with T4 DNA ligase. The dimer was purified from an agarose gel (Supplementary Figure S1) and was cloned into the EcoRI site of a pBlueScript SK- vector. Individual clones were screened by enzyme digestion and PCR to identify those that had the tandem repeat in phase, and then verified by sequencing (Supplementary Figure S2). For the circular permutation synthesis, seven sets of forward and reverse primers were used to produce a series of 150 bp nucleosomal DNAs that position the T_{11}-tract at seven different SHLs along an NCP, at 0 (dyad), −1, −2, −3, −4, −5 and −6 (Supplementary Figure S3).

Nucleosome core particle reconstitution and assay by hydroxyl radical footprinting

To determine the optimal conditions for NCP reconstitution, the 150-bp DNA duplexes were 5′-end labeled and titrated with NCPs isolated from chicken erythrocytes under high salt conditions that promote nucleosomal DNA exchange, followed by lowering of the salt concentration and thermal annealing (18). Electrophoresis on a native gel showed that about 95% of the 150-mer DNAs could be incorporated into a single NCP band at an NCP:DNA ratio of 600:1 (Supplementary Figure S4). To determine the rotational and translational setting of the DNA on the nucleosome, the reconstituted NCPs were subjected to HO· footprinting. The HO· cleavage pattern exhibited a very pronounced 10–11 bp periodicity, indicating that the 150-mer DNAs were rotationally phased. The cleavage pattern was mapped onto the DNA sequence by alignment with the Maxam-Gilbert G reaction bands (Figure 3).

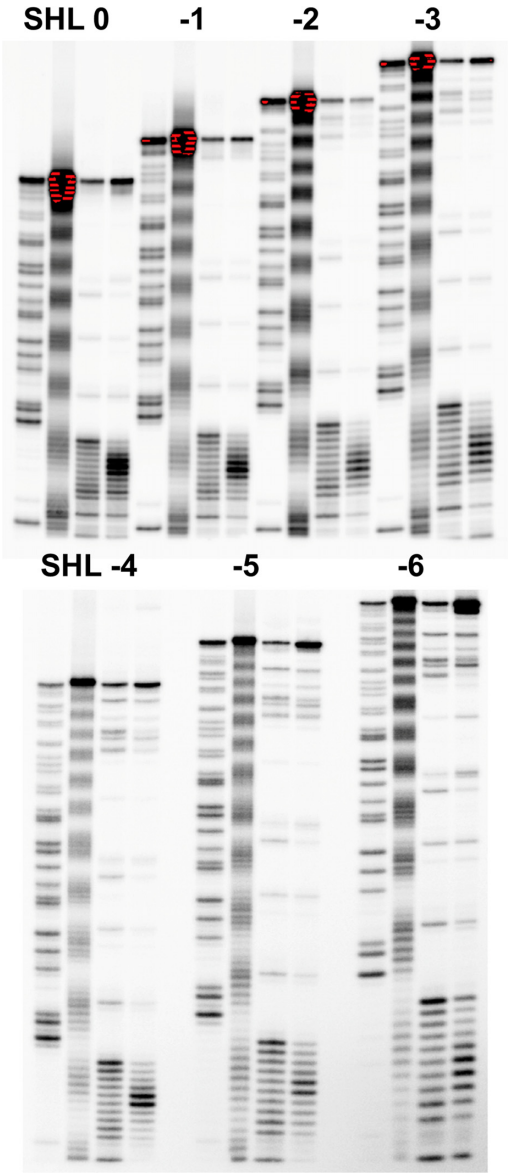

Figure 3. PAGE analysis of the hydroxyl radical footprinting of the nucleosome core particles (NCPs) and assay of CPD formation in free and nucleosome-bound DNA. The first lane of each set of four lanes is the Maxam Gilbert G ladder, the second lane is the HO· footprint of the DNA in the NCP, the third lane is the CPD-specific T4-pdg-treated UVB-irradiated free DNA, and the fourth lane is the CPD-specific T4-pdg-treated irradiated nucleosome-bound DNA.

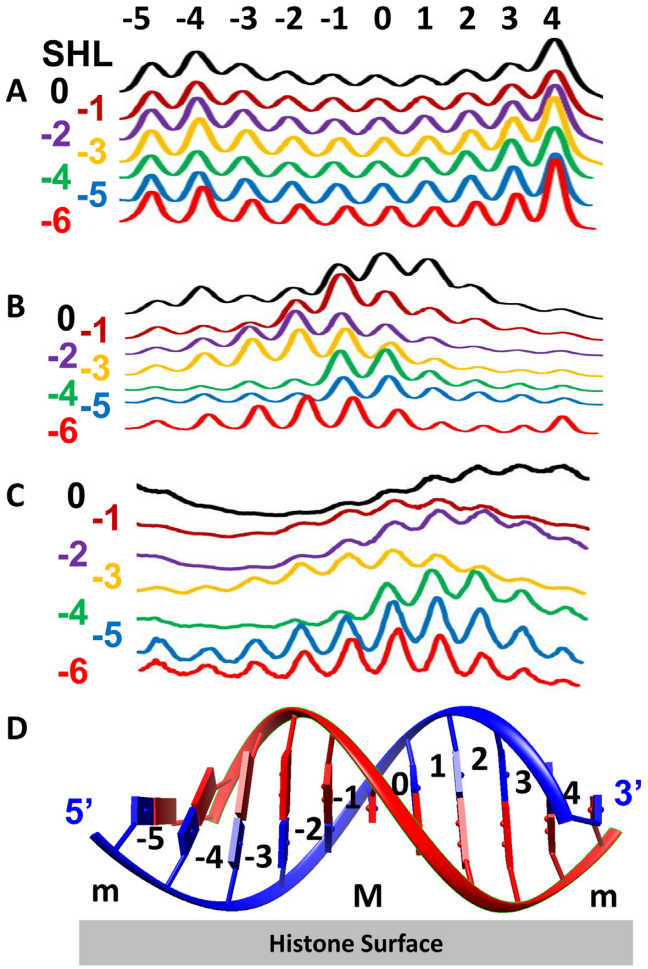

Figure 4. Footprinting and CPD patterns in nucleosome-bound DNA compared to the CPD pattern in free DNA. Traces of the T_{11}-tract section of the lanes in Figure 3 of (**A**) CPD formation in free DNA, (**B**) CPD formation in nucleosome bound DNA and (**C**) HO· cleavage in nucleosome bound DNA. The numbers to the left are the SHLs of the T_{11}-tract, while the numbers above correspond to the position of the cleaved T in the T_{11}-tract in which the 0 position is expected to align with the dyad in the SHL 0 construct as shown in (**D**). M and m refer to where the major and minor grooves face the nucleosome surface.

The HO· footprinting pattern was used to verify the translational position of the T_{11}-tract based on the expectation that the periodic modulation of the HO· cleavage pattern would only be apparent where the DNA was in direct contact with the histone core. Hydroxyl radical preferentially cleaves DNA at sites where the sugar phosphate backbone is most exposed and faces away from the histone surface, and is inhibited where it faces the histone surface. For the dyad position, one can clearly see the expected six repeats of HO· cleavage bands above (to the 3′-side of) the band at the T_{11}-tract, with the last band appearing at the edge of the large uncleaved band corresponding to full length DNA. The number of repeats increased by one as the T_{11}-tract was moved an additional 10 bp toward the 5′-end. When the T_{11}-tract was positioned at SHL −6, 12 repeats are observed. These results, coupled with the observation of a single nucleosomal band in the electrophoresis gel following nucleosomal DNA exchange (Supplementary Figure S4) indicates that the 150-mer DNA's were all largely adopting a single, centered translational position that maximizes histone–DNA contacts. Had the DNA shifted by 10 bp to either side, contact between one turn of the helix and the nucleosome would have been lost, which would be thermodynamically unfavorable.

There were differences, however, in the alignment of the HO· cleavage bands with the T-tract sequence at different SHLs (Figures 4 and 5A). The HO· cleavage band pattern for each SHL could be fit to a Gaussian function with the average position of the band maximum at +1 ± 1 relative to

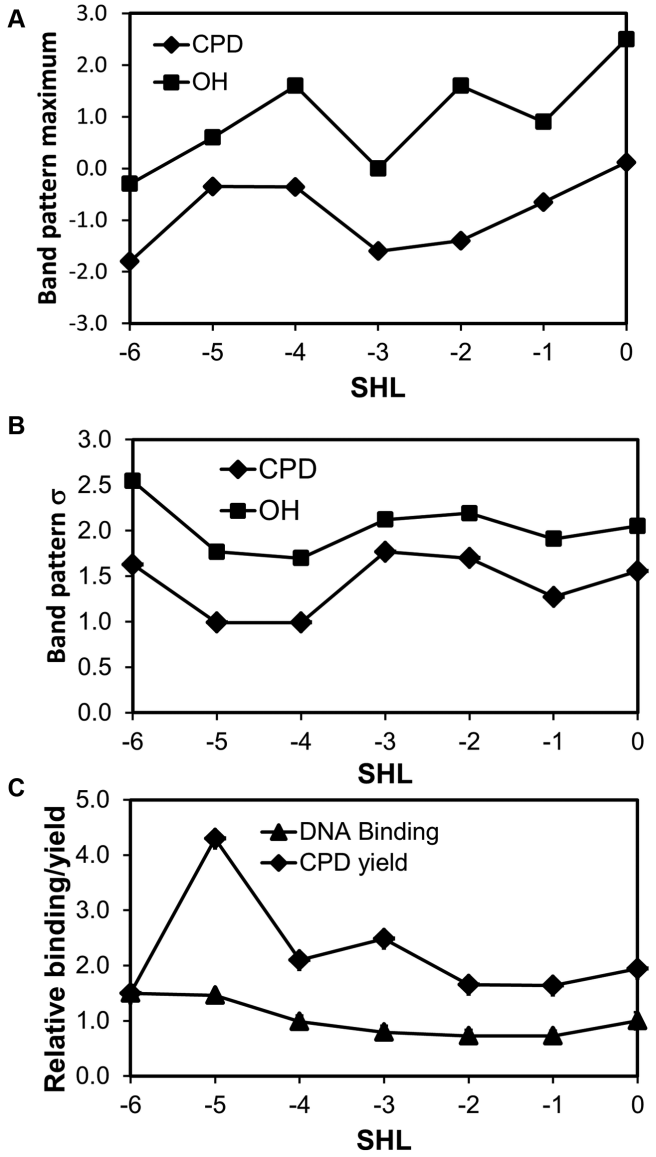

Figure 5. Quantification of the CPD and footprinting band patterns, relative CPD yields and nucleosomal DNA binding affinities. (**A**) Comparison of the position of maximum CPD formation and HO· cleavage in the T_{11}-tracts of the nucleosome-bound DNA as a function of SHL calculated from Gaussian analysis of the pattern of bands in Figure 4. (**B**) Comparison of the standard deviation of the Gaussian function used to fit the CPD and HO· cleavage patterns. (**C**) Yield of CPDs in the NCP relative to free DNA for the T_{11}-tracts as a function of SHL, together with the binding affinity of the DNA for the nucleosome relative to SHL 0.

the base pair assigned as 0 in the T_{11}-tract, The spread of cleavage bands had an average standard deviation σ of 2.0 ± 0.3, corresponding to a band width at half peak height of 2.355 σ or 4.8 ± 0.7 nucleotides (nt). Previous HO· footprinting of a repetitive TG motif-containing nucleosome (13) and one containing the Widom 601 sequence (19) also showed a variation of two or more in the position of maximum cleavage from that expected for a 10–11 bp repeat. The variability in the position of the HO· cleavage band maxima could be due to differences in the precise translational position and hence rotational position of the nucleosomal DNA at different SHLs caused by the T_{11}-tract. The variability could also be due to differences in DNA conformation or interactions with histone tails at different SHLs. Removing the histone tails, however, has not been previously found to alter the HO· footprinting pattern, but the point to which the tails were truncated was not indicated (20).

T=T CPD distribution within T_{11} tracts as a function of SHL

Free or nucleosome bound 150-mer DNA duplexes were irradiated with broadband UVB light centered at 312 nm light at 0°C to produce the cis-syn T=T CPDs within the T_{11}-tracts. The irradiation time was chosen to maximize signal to noise while still maintaining the pattern observed at lower doses (Supplementary Figures S5 and 6). The nucleosome bound samples were then phenol extracted to remove histone core proteins, ethanol precipitated and incubated with T4 pyrimidine dimer glycosylase or T4-pdg (formerly T4 endonuclease V) to reveal the locations of the CPDs. T4-pdg is a glycosylase that hydrolyzes the N-glycosidic linkage of the 5′-T of the CPD, and then causes strand cleavage by an associated lyase activity to first yield a 5′-phosphate terminated end by a β-elimination reaction, followed by formation of a 3′-phosphate terminated end by a slower δ-elimination reaction (21). These are the same ends that are produced by the Maxam-Gilbert reactions, and the 3′-phosphate is the major end produced by HO··-mediated hydrogen abstraction at C5 and C4 of the sugar ring (22). To ensure complete δ-elimination of the sugar, the samples were further incubated with 1 M piperidine at 90°C for 5 min. The samples were sequentially loaded in time so that the cleavage bands at the T_{11}-tracts ran at approximately the same position on the gel (Figure 3). Because hot piperidine is also known to cause cleavage at (6–4) and Dewar photoproducts (23), we treated an irradiated T_{11}-tract containing 41-mer under the same conditions without T4-pdg, and found no additional bands (Supplementary Figure S5), confirming that the observed patterns in free DNA were due solely to CPDs. This is consistent with the fact that TT (6–4) and Dewar photoproducts form with 7 and 0.3%, respectively, of the frequency of CPDs with UVB light (24). These photoproducts are expected to form even less in nucleosomes, which are known to suppress (6–4) products about 6-fold compared to internucleosomal or linker DNA (25).

The CPD cleavage band patterns in free and nucleosome bound DNA were completely different and showed essentially the opposite intensity pattern (Figure 4). In free DNA, all seven T_{11}-tract positions show the same T=T CPD band pattern, with the highest CPD frequency at the 3′-end, decreasing to a minimum in the center, and increasing slightly at the 5′ end, as previously observed by others in T-tracts of various lengths (26,27). In nucleosome bound DNA, the band pattern was reversed, with the CPD frequency highest in the middle of the T-tract and tapering off toward the 5′- and 3′-ends. The pattern of CPD cleavage bands within the T_{11}-tracts at all seven SHLs could be fit to a Gaussian function with an average maximum band position at −0.9 ± 0.7 relative to the base pair assigned as 0, and with a σ of 1.4 ± 0.3 (Figure 5A and B). While almost all of the CPD cleavage bands fit a Gaussian, outlier CPD cleavage bands were observed at −4 in the T_{11}-tract of the dyad NCP and at

+4 in the −6 NCP, which map to positions in a nucleosome crystal structure (1AOI.pdb) that are in close contact with paired loops in histone folds.

The position of the CPD band pattern maximum within the T_{11}-tracts in the NCP also varied with translational position much like that of the HO· cleavage band patterns. A variation in the position of maximum CPD formation with translational position has also been observed for irradiated chromatin, but with a different average position (5). The average maximum position of CPD formation in the T_{11}-tracts was 1.8 ± 0.7 nucleotides to the 5′-side of the site of the average maximum position of HO· cleavage. For most translational positions, CPD formation tracked with HO· cleavage (Figure 5A), with the exception of the dyad and SHL −2 positions which showed differences of 2.4 and 3 nt between sites of maximum CPD formation and HO· cleavage. Interestingly, the standard deviations for the Gaussian fits of the CPD band patterns tracked very closely with those for HO· cleavage and did not show any large deviation at the dyad and the SHL −2 positions (Figure 5B).

The progressive change of the position of maximal cleavage toward the 5′-end in the nucleosomal DNA's with an increase in the translational position away from the dyad can be explained in part by the fact that the helical repeat is not exactly 10 bp/turn in the nucleosome. Inspection of the crystal structure of a 147-mer DNA nucleosome (1kx5.pdb) shows that the base pair orientation equivalent to that at the dyad occurs at −10, −31, −52 and −73, which could explain the overall shift of the position of maximum CPD formation from +0.1 at the dyad to −2 for the SHL −6 T-tract (28). The variation in the position of maximum CPD formation or HO· cleavage is not linear with translational position, however, suggesting that the T-tract itself may lead to adjustments in the actual rotational and translational positioning of the T-tracts on the histone core particle as a function of position.

The 5′-shift in the position of the maximum CPD formation relative to the HO· cleavage is in accord with what was previously observed in a naturally occurring DNA sequence containing T-tracts of various lengths (9). This is different from what has previously been observed for non-T-tract sequences, where the maximum of CPD formation and HO· cleavage closely coincided (11,29). The frequency of CPD formation in these sequences was found to correlate with the amplitude of nucleotide motion as inferred from temperature factors of the nucleotides in the crystal structures of nucleosomes. The temperature factors in turn correlate with the degree to which the backbone faces away from the protein surface, and hence the sites most accessible to HO· (11). The average 1.8 bp shift in position of the maximum CPD cleavage in T-tracts relative to HO· cleavage would thus appear to be due to a difference in the DNA conformation, flexibility or histone interactions between T-tracts and heterogeneous DNA.

In the crystal structure of a nucleosome containing a T_{16}-tract (2FJ7.pdb) (30) the temperature factors for the individual T's in the T_{16}-tract paralleled those seen in non-T-tract DNA in a nucleosome (Supplementary Figure S7A), suggesting that something other than nucleotide dynamics was controlling CPD formation frequency. It was noted that the minor groove of the T_{16}-tract was significantly narrowed in the crystal structure, suggesting that this conformation might be an important determinant. Previous molecular dynamics studies of CPD formation have suggested that CPD formation is most favorable when the distance between the centroids of the C5–6 bonds of adjacent thymidines and the improper torsion angle (T_nC5–C6-$T_{n+1}C6$–C5) fall within the range of 0 to 3.6 Å and 0 to 48° (31). Analysis of these parameters within the T_{16}-tract show that among all the TT sites, only the T_{251}–T_{252} site comes close to these values, with values of 3.7 Å and 38° (Supplementary Figure S7B). This site corresponds to the −1 and 0 positions relative to the translated dyad axis, and occurs 2 nt to the 5′-of the position of the maximum nucleotide temperature factor at positions +1 and +2. The next closest site is 252 and 253 which had values of 4.1 Å and 24°. Thus it is possible that the T-tract adopts a slightly different structure from heterogeneous DNA that shifts CPD formation frequency to the 5′-side.

Binding affinity as a function of T-tract translational position

If the observed differences in CPD formation and HO· cleavage patterns at the T-tracts at difference SHLs were due to different alignments of the T_{11}-tract, then one might expect that they could have an effect on the binding affinity of the DNA. To test this possibility, we determined the binding affinity of the various DNAs relative to the DNA at SHL 0 by previously described competition experiments (13,16). Briefly, the concentration of chicken nucleosomal DNA required to reduce the binding of radiolabeled SHL 0 DNA to 50% was first determined by titration. The other radiolabeled DNAs were incubated with this same amount of chicken nucleosomal DNA and the fraction bound was determined. The results are graphed in Figure 5C, and show that the relative binding affinity dropped slightly from 1 for SHL 0 to 0.7 for SHL −1 and −2, and then increased from 0.8 for SHL −3 to 1 for SHL −4 and then to 1.5 for SHL −5 and −6. The relative binding affinities are what one might expect for the presence of a destabilizing sequence which would cause least disruption of binding when it is placed at the end of the nucleosomal DNA. The observed binding trend, however, does not appear to correlate with the observed CPD and HO· cleavage patterns.

CPD yield as a function of T-tract SHL

While the study of individual T_{11}-tract DNAs revealed differences in the pattern of CPD formation as a function of SHL, it did not reveal whether or not the overall formation of CPDs at a particular SHL was enhanced or inhibited. To determine this, we first irradiated radiolabeled SHL 0 and −1 DNAs with radiolabeled 41-mer DNA before and after assembly with nucleosomal core particles, where it was expected that the 41-mer DNA would remain free in solution under both conditions. Then a mixture of SHL 0, −2, −4 and −6 DNA was irradiated before and after assembly into a nucleosome, and the same was done for a mixture of SHL −1, −3 and −5 DNA. After quantifying and normalizing the band volumes, the CPD yields could be calculated as a function of translational position relative to free DNA (Figure 5C). As can be seen the CPD yield at SHL 0 was greater

than for free DNA and then dramatically rose 4.5-fold for SHL −5, after which it dropped back down to 1.5-fold for SHL −6. The results are generally in accord with what has been observed for CPD formation in mixed sequence NCPs in which CPD yield increased on going from the dyad to the 5′-end (5), though this may also reflect some sort of sequence bias. There does not, however, appear to be any correlation between CPD yield and the position of maximum for CPD formation in the T11-tracts as a function of translational position.

Temperature study of T=T CPD formation in nucleosomes at the dyad and SHL −6

Because it is known that the frequency of CPD formation within a T-tract in free DNA is temperature dependent (26), we examined the effect of temperature on CPD formation in both free and nucleosome bound DNA. First, a 41 bp free DNA duplex containing a T_{11}-tract in the center was irradiated with UVB light at 0, 10, 20, 30 and 40°C. The CPD band pattern shifted from one with a major peak at the 3′-end to a more even distribution of peaks as the temperature increased (Supplementary Figure S8) in accord with a previous study on T-tracts of various different lengths (26). This change was attributed to a shift from the T-tract structure to a normal B DNA structure at higher temperatures.

Since the greatest difference in CPD band patterns for the nucleosome free 41-mer was observed at 0 and 40°C, the free and nucleosome bound DNA were irradiated with UVB light at these two temperatures. Only the DNAs with the T_{11}-tract at the dyad and −6 SHL positions were subjected to this temperature study because they represent two extreme positions of conformational flexibility in a nucleosome (32). As expected, the CPD band pattern in the two nucleosome-free DNAs changed in the same way as in the 41-mer duplex when heated from 0 to 40°C, in which the major bands were at the 3′-end of the T-tract at 0°C and more evenly distributed at 40°C, though favoring the 5′-side (Figure 6). The bias for the 5′-side may be due to the fact that CPD formation was more efficient at 40°C than at 0°C, as evidenced by the decrease in the percentage uncleaved substrate, which would favor shorter end-labeled fragments resulting from a greater number of multiple cleavages per strand. In contrast, CPD formation at both the dyad and SHL −6 positions in the nucleosome showed similar Gaussian band patterns at 0°C that did not change significantly upon heating to 40°C, except perhaps for a small shift in the position of the maximum peak to the 5′-side, possibly due to the increased CPD formation efficiency. For the dyad NCP, the Gaussian band pattern was centered at +0.2 at 0°C and shifted slightly 5′ to −0.3 upon heating to 40°C, while σ also increased slightly from 1.3 to 2.1. Likewise, the center of the Gaussian band pattern for SHL −6 NCP moved slightly 5′ from −1.5 to −1.9 with a similar small increase in σ from 1.3 to 1.8. The small changes in the pattern of CPD formation in the NCP with an increase in temperature suggest that the flexibility of the DNA does not increase significantly with temperature. The small changes also suggest that the 5′-end of the nucleosomal DNA is not much more flexible than that at the dyad, and remains largely bound to the histone core even at 40°C.

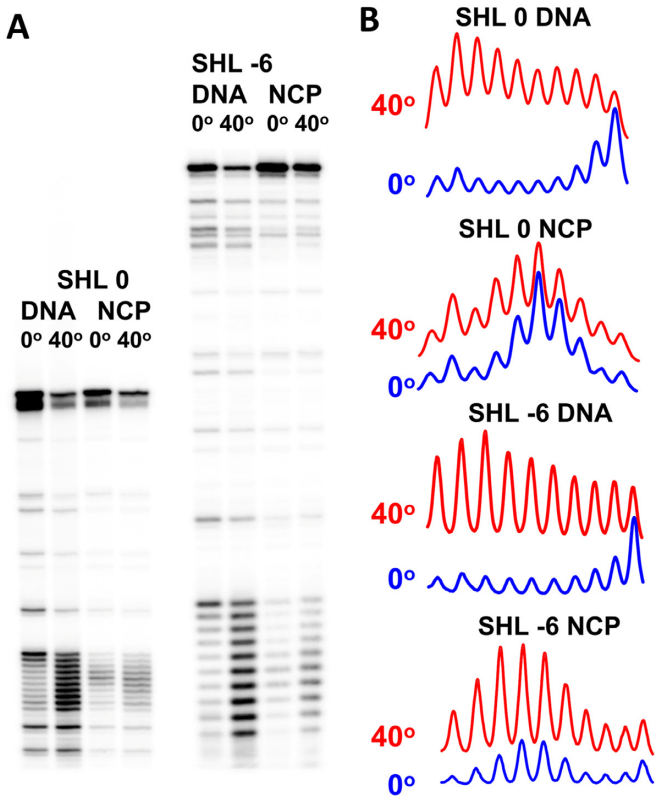

Figure 6. PAGE analysis of the effect of temperature on the frequency of CPD formation in T_{11}-tracts in free and nucleosome-bound DNA. (**A**) Radioimage of the PAGE gel of the T4-pdg cleavage products of irradiated free (DNA) and nucleosome-bound DNA (NCP) at SHL 0 and −6, at 0 and 40°C, and (**B**) scans of the lanes at the sites of the T_{11}-tracts.

Minicircle DNA mimic of nucleosomal DNA

While it is clear from this study of T_{11}-tracts and the previous one of various sized T-tracts in a section of promoter DNA (9) that the nucleosome can dramatically alter CPD formation in T-tracts, it is not clear to what extent that this is due to the histone proteins or to DNA bending. In a previous study, lambda repressor was used to constrain the formation of a protein-free DNA loop and show that DNA bending alone can modulate CPD formation (7). In that study the site of maximum of CPD formation coincided with the site of maximum DNAse I cleavage which has been shown to occur 1–2 bases to the 3′-side of the dyad in a nucleosome phased by TG motifs (33). The exact shape, curvature and rotational phasing of the DNA in the lambda repressor system is unknown, however, and therefore cannot be directly correlated with NCPs. We therefore decided to investigate CPD formation in the T_{11}-tract of an 80 bp circular DNA section of the same rotationally phased sequence we used in the nucleosomal DNA studies to mimic one turn of the nucleosomal DNA. In the nucleosome crystal structure 1kx5.pdb, one complete turn of DNA around the nucleosome corresponds to about 79 bp (28). We included one more bp in our sequence so as not to interrupt the 10 bp repeat of the TG motifs used to rotationally phase the DNA (Figure 7).

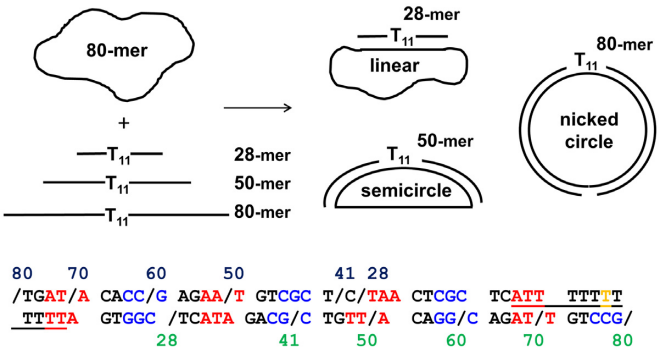

Figure 7. Minicircle approach to determine the effect of bending on CPD yield in T_{11}-tracts. A single strand 80-mer corresponding to one full turn of the central section of the 150-mer nucleosomal DNA that is complementary to the T_{11}-tract containing sequence shown was circularized by ligation using a ligation scaffold. The 80-mer was then annealed to increasingly long 5′-radiolabeled complementary strands containing a centrally located T_{11}-tract to form DNA duplex sections with different degrees of bending as a result of tension from the remaining single strand. The 5′- and 3′-ends of the complementary sequences used are indicated with a forward slash. Other features are as described in the Figure 2 caption.

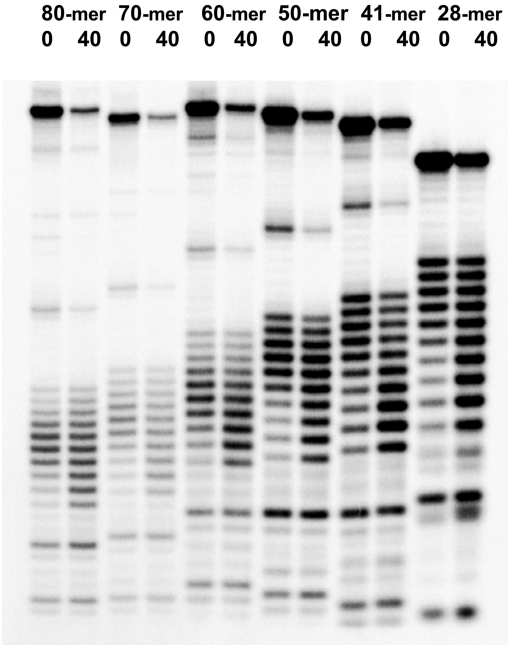

Figure 8. PAGE assay of CPD formation in the minicircular DNAs as a function of duplex length and temperature. The radiolabeled minicircular DNAs were irradiated with UVB light at 0 and 40°C, treated with T4-pdg and electrophoresed. The samples were loaded at different time intervals so as to have the T_{11}-tract cleavage bands appear at roughly the same location in the gel.

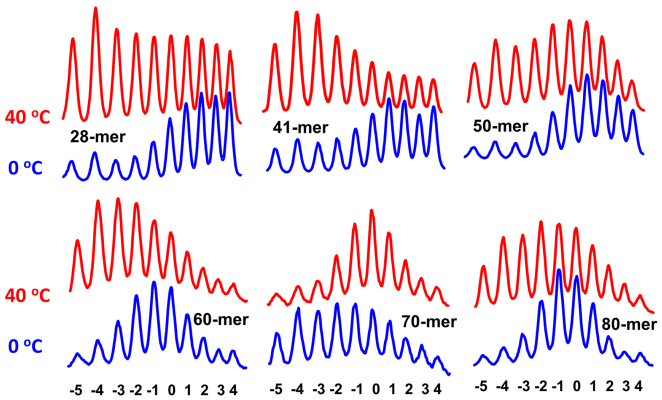

Figure 9. Frequency of CPD formation in the minicircles as a function of duplex length and temperature. The lanes in Figure 8 were scanned and the CPD formation patterns for the T_{11}-tracts for a given duplex length at 0°C (blue) and 40°C (red) are stacked on each other.

The 80-mer single strand circular DNA complementary to the T_{11}-tract was prepared by ODN templated-directed ligation of a synthetic single strand 80-mer. The circular DNA was isolated and hybridized (Supplementary Figure S9) to complementary strands 28, 41, 50, 60, 70 and 80 nt in length with the T_{11}-tract near the center of each sequence (Figure 7). We expected that the single stranded section of DNA would generate a bending force on the double strand DNA (dsDNA) section, when the length of the dsDNA segment exceeded the length of the remaining single strand, much like in a molecular vise (34). We therefore expected that the DNA duplex in a minicircle hybrid formed from a short DNA would remain linear, whereas the DNA duplex in hybrids formed with the longer DNAs would become increasingly bent with length, and that this would be reflected in the CPD distribution in the T_{11}-tract. To determine this, the hybrid DNA minicircles were then UVB irradiated at 0 and 40°C and then assayed for CPDs by T4-pdg (Figures 8 and 9).

At 0°C, the pattern of CPD formation for the 80-mer minicircle hybridized to the 28-bp DNA was similar to that for the 41- or 150-bp free DNA in that the maximum CPD yield was at the 3′-end, except that the distribution of peaks was broader. As the length of the duplex section increased to 41 and 50, the CPD pattern began to shift slightly toward the center with maxima at +2.0 and +1.4, respectively, relative to the 0 position corresponding to where the dyad axis would be in the nucleosome. When the segment reached 60, 70 and 80 bp, the CPD maxima shifted to the middle of the T tract, with maxima at positions −0.8, 0 and −0.5, respectively, which are close to the average of −0.9 observed for the nucleosome bound DNAs (Figure 10A). In addition, the standard deviation of the Gaussian fits became narrower, decreasing linearly from 2.5 for the 28-mer to 1.5 for the 80-mer, which was also close to the average of 1.4 seen for the nucleosome (Figure 10B). The close correlation between what was observed in the nucleosome and in the minicircle suggests that the minicircle is adopting an average structure with the same curvature and rotational phase as in the nucleosome, and that these two parameters are sufficient to explain the modulation of CPD formation by the nucleosome.

At the higher temperature of 40°C, the in phase 28-mer hybrid minicircle gave a fairly even pattern of CPDs, with a bias for the five-side (Figures 8 and 9), as was observed for the T_{11}-tracts of the nucleosome-free SHL 0 and −6 DNA duplexes at the same temperature (Figure 6B). The CPD pattern for the 41-mer hybrid minicircle could be fit to a Gaussian with a maximum at −3.3, while the maxima for the 60-, 70- and 80-mer hybrid minicircles moved

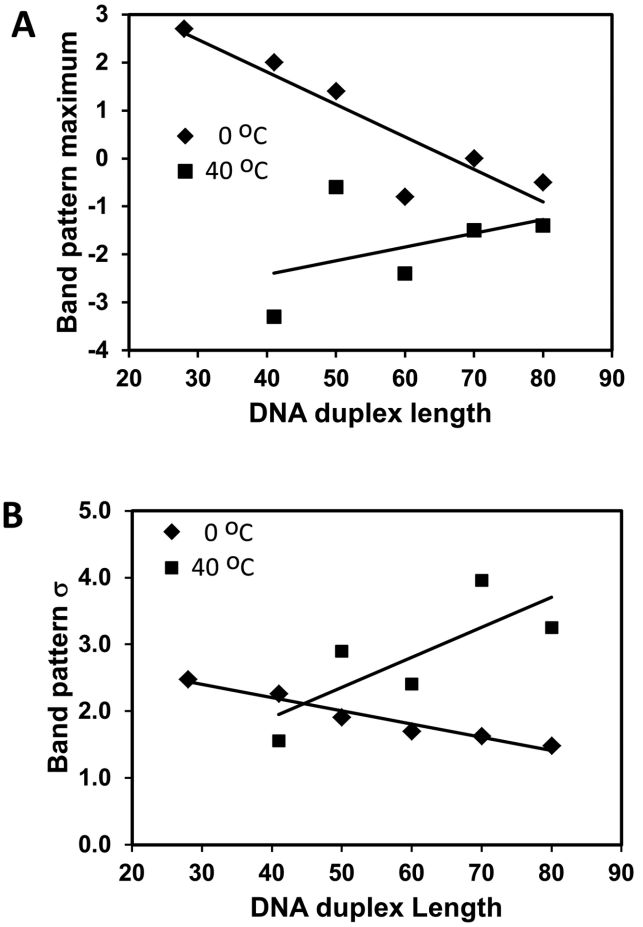

Figure 10. Plots of Gaussian fits to the CPD cleavage patterns for the minicircles as a function of duplex length. (**A**) A plot of the position of maximum CPD formation from fitting the cleavage patterns to a Gaussian function. (**B**) The standard deviation of the Gaussian fits.

increasingly toward the center with maxima at −2.4, −1.5 and −1.4 (Figure 10A). The position of maximum CPD formation at 40°C came within about one base to the 5′-side of that observed at 0°C in the 80-mer hybrid. Again, this may be attributed to the higher cleavage efficiency at 40°C which resulted in a greater percentage of multiple cleavages that favors shorter end-labeled fragments. The 50-mer hybrid minicircle did not follow the general trend and for reasons not understood at this time had a maximum at −0.6 at 40°C, which was much more toward the 3′-end than for any of the other minicircles. The standard deviation of the Gaussian fits was greater at 40°C than observed at 4°C, and in contrast to 4°C, generally increased rather than decreased on going from the 41-mer to the 80-mer hybrid minicircles (Figure 10B), possibly due to the more extensive cleavage which favors shorter end-labeled cleavage products.

The behavior of our fully duplex 80-mer minicircle is consistent with previous studies showing that covalently closed circular DNAs as small as 70 bp with the lowest superhelical density can adopt circular forms without kinking as judged from cryo-EM and enzymatic probe studies. By using sensitivity to BAL31 and S1 digestion, DNAs of 84–86 bp in length were found to form kink-free covalently closed circular DNAs (35). Because the fully complementary 80-mer DNA that we used contained a nick, it is possible that it could have kinked at this site. Kinking at one end of a circular DNA, however, would increase the curvature of the opposite end and would be expected to lead to a second kink opposite the first kink (36). We see no evidence of such a kink which would have caused significant disruption to the CPD pattern in the T_{11}-tract which is almost directly opposite the nick in the 80-mer circular DNA duplex. Likewise, a cryo-EM study of 94-bp DNA circle containing nicks at opposite ends showed no significant evidence of such double kinking (37). T-tracts themselves have been found to be highly flexible by single molecule experiments probing looping (38) and DNA cyclization (39).

To verify that the pattern of CPD formation was related to the rotational phasing, and not some other effect, we constructed an 80-mer nicked duplex in which the T_{11}-tract was out of phase by one half a turn (Supplementary Figures S10 and S11). When this minicircle was irradiated at 0°C, the CPD pattern completely changed. As expected, CPD formation was minimal at the center of the T-tract and maximal at the ends. When irradiated at 40°C, the CPD pattern was somewhat more even, but still favored the ends.

CONCLUSION

We have shown by way of CPD formation that the nucleosome is capable of modifying the conformation of T_{11}-tracts at all SHLs, including −6. Considering that the T_{11}-tract at SHL −6 is only one turn away from where the DNA exits the nucleosome, and is therefore the least constrained, it must be quite bendable to bind. We have also shown that the pattern of CPD formation in nucleosomes can be reproduced with a nicked circular 80-mer DNA, corresponding to a full turn of DNA around the nucleosome, that contains phased TG-motifs. The great similarity between the pattern of CPD formation in the nucleosome and in the minicircle suggests that the DNA in the minicircle is adopting the same rotational phase and curvature as in the nucleosome, and is not freely rotating about the helical axis or kinking. This conclusion was further supported by the observation that changing the phase of the T_{11}-tract changed the CPD pattern. Such a rotationally phased unkinked 80-mer mini-circular duplex should therefore be a good model for assessing the effect of DNA bending on hydrolytic deamination of cytosine-containing CPDs, as well as other reactions of nucleosomes. The ability of the T_{11}-tract to smoothly bend within the 80-mer minicircle is in accord with previous studies that found that T-tracts enhanced the bendability of DNA (39), and further begs an answer to the question of why T-tracts are excluded from nucleosomes in yeast (40,41). The bend-dependent pattern of CPD formation within the T_{11}-tract might also be useful for reporting on the magnitude and phasing of bends in looped DNA structures *in vitro* and *in vivo*. Rotationally phased mini-circular DNA's might also find important applications for nano-scale construction and assembly of spatially organized materials.

SUPPLEMENTARY DATA

Supplementary Data are available at NAR Online.

ACKNOWLEDGEMENTS

We thank Vincent Cannistraro and Santhi Pondugula for advice and help with various experimental procedures. We also thank Stephen Lloyd for a T4-pdg clone.

FUNDING

National Institutes of Health (NIH) [R01-CA40463]. Funding for open access charge: NIH R01-CA40463.
Conflict of interest statement. None declared.

REFERENCES

1. Brash,D.E. (2015) UV signature mutations. *Photochem. Photobiol.*, **91**, 15–26.
2. Pfeifer,G.P. and Besaratinia,A. (2012) UV wavelength-dependent DNA damage and human non-melanoma and melanoma skin cancer. *Photochem. Photobiol. Sci.*, **11**, 90–97.
3. Ikehata,H. and Ono,T. (2011) The mechanisms of UV mutagenesis. *J. Radiat. Res.*, **52**, 115–125.
4. Pfeifer,G.P., You,Y.H. and Besaratinia,A. (2005) Mutations induced by ultraviolet light. *Mutat. Res.*, **571**, 19–31.
5. Gale,J.M. and Smerdon,M.J. (1988) Photofootprint of nucleosome core DNA in intact chromatin having different structural states. *J. Mol. Biol.*, **204**, 949–958.
6. Pehrson,J.R. (1989) Thymine dimer formation as a probe of the path of DNA in and between nucleosomes in intact chromatin. *Proc. Natl. Acad. Sci. U.S.A.*, **86**, 9149–9153.
7. Pehrson,J.R. and Cohen,L.H. (1992) Effects of DNA looping on pyrimidine dimer formation. *Nucleic Acids Res.*, **20**, 1321–1324.
8. Liu,X., Mann,D.B., Suquet,C., Springer,D.L. and Smerdon,M.J. (2000) Ultraviolet damage and nucleosome folding of the 5S ribosomal RNA gene. *Biochemistry*, **39**, 557–566.
9. Schieferstein,U. and Thoma,F. (1996) Modulation of cyclobutane pyrimidine dimer formation in a positioned nucleosome containing poly(dA.dT) tracts. *Biochemistry*, **35**, 7705–7714.
10. Finch,A.S., Davis,W.B. and Rokita,S.E. (2013) Accumulation of the cyclobutane thymine dimer in defined sequences of free and nucleosomal DNA. *Photochem. Photobiol. Sci.*, **12**, 1474–1482.
11. Song,Q., Cannistraro,V.J. and Taylor,J.-S. (2014) Synergistic modulation of cyclobutane pyrimidine dimer photoproduct formation and deamination at a TmCG site over a full helical DNA turn in a nucleosome core particle. *Nucleic Acids Res.*, **42**, 13122–13133.
12. Pfeifer,G.P., You,Y.H. and Besaratinia,A. (2005) Mutations induced by ultraviolet light. *Mutat. Res.*, **571**, 19–31.
13. Shrader,T.E. and Crothers,D.M. (1989) Artificial nucleosome positioning sequences. *Proc. Natl. Acad. Sci. U.S.A.*, **86**, 7418–7422.
14. Levene,S.D., Wu,H.M. and Crothers,D.M. (1986) Bending and flexibility of kinetoplast DNA. *Biochemistry*, **25**, 3988–3995.
15. Ryabinina,O.P., Minko,I.G., Lasarev,M.R., McCullough,A.K. and Lloyd,R.S. (2011) Modulation of the processive abasic site lyase activity of a pyrimidine dimer glycosylase. *DNA Repair (Amst)*, **10**, 1014–1022.
16. Jayasena,S.D. and Behe,M.J. (1989) Competitive nucleosome reconstitution of polydeoxynucleotides containing oligoguanosine tracts. *J. Mol. Biol.*, **208**, 297–306.
17. Svedruzic,Z.M., Wang,C., Kosmoski,J.V. and Smerdon,M.J. (2005) Accommodation and repair of a UV photoproduct in DNA at different rotational settings on the nucleosome surface. *J. Biol. Chem.*, **280**, 40051–40057.
18. Kosmoski,J.V. and Smerdon,M.J. (1999) Synthesis and nucleosome dtructure of DNA containing a UV photoproduct at a specific site. *Biochemistry*, **38**, 9485–9494.
19. Syed,S.H., Goutte-Gattat,D., Becker,N., Meyer,S., Shukla,M.S., Hayes,J.J., Everaers,R., Angelov,D., Bednar,J. and Dimitrov,S. (2010) Single-base resolution mapping of H1-nucleosome interactions and 3D organization of the nucleosome. *Proc. Natl. Acad. Sci. U.S.A.*, **107**, 9620–9625.
20. Hayes,J.J., Clark,D.J. and Wolffe,A.P. (1991) Histone contributions to the structure of DNA in the nucleosome. *Proc. Natl. Acad. Sci. U.S.A.*, **88**, 6829–6833.
21. Latham,K.A. and Lloyd,R.S. (1995) Delta-elimination by T4 endonuclease V at a thymine dimer site requires a secondary binding event and amino acid Glu-23. *Biochemistry*, **34**, 8796–8803.
22. Balasubramanian,B., Pogozelski,W.K. and Tullius,T.D. (1998) DNA strand breaking by the hydroxyl radical is governed by the accessible surface areas of the hydrogen atoms of the DNA backbone. *Proc. Natl. Acad. Sci. U.S.A.*, **95**, 9738–9743.
23. Kan,L.S., Voituriez,L. and Cadet,J. (1992) The Dewar valence isomer of the (6-4) photoadduct of thymidylyl-(3'-5')-thymidine monophosphate: formation, alkaline lability and conformational properties. *J. Photochem. Photobiol. B*, **12**, 339–357.
24. Douki,T. and Cadet,J. (2001) Individual determination of the yield of the main UV-induced dimeric pyrimidine photoproducts in DNA suggests a high mutagenicity of CC photolesions. *Biochemistry*, **40**, 2495–2501.
25. Mitchell,D.L., Nguyen,T.D. and Cleaver,J.E. (1990) Nonrandom induction of pyrimidine-pyrimidone (6-4) photoproducts in ultraviolet-irradiated human chromatin. *J. Biol. Chem.*, **265**, 5353–5356.
26. Lyamichev,V. (1991) Unusual conformation of (dA)n. (dT)n-tracts as revealed by cyclobutane thymine-thymine dimer formation. *Nucleic Acids Res.*, **19**, 4491–4496.
27. Suter,B., Schnappauf,G. and Thoma,F. (2000) Poly(dA.dT) sequences exist as rigid DNA structures in nucleosome-free yeast promoters in vivo. *Nucleic Acids Res.*, **28**, 4083–4089.
28. Davey,C.A., Sargent,D.F., Luger,K., Maeder,A.W. and Richmond,T.J. (2002) Solvent mediated interactions in the structure of the nucleosome core particle at 1.9 a resolution. *J. Mol. Biol.*, **319**, 1097–1113.
29. Song,Q., Cannistraro,V.J. and Taylor,J.S. (2011) Rotational position of a 5-methylcytosine-containing cyclobutane pyrimidine dimer in a nucleosome greatly affects its deamination rate. *J. Biol. Chem.*, **286**, 6329–6335.
30. Bao,Y., White,C.L. and Luger,K. (2006) Nucleosome core particles containing a poly(dA.dT) sequence element exhibit a locally distorted DNA structure. *J. Mol. Biol.*, **361**, 617–624.
31. Law,Y.K., Azadi,J., Crespo-Hernandez,C.E., Olmon,E. and Kohler,B. (2008) Predicting thymine dimerization yields from molecular dynamics simulations. *Biophys. J.*, **94**, 3590–3600.
32. Dobrovolskaia,I.V. and Arya,G. (2012) Dynamics of forced nucleosome unraveling and role of nonuniform histone-DNA Interactions. *Biophys. J.*, **103**, 989–998.
33. Li,Q. and Wrange,O. (1993) Translational positioning of a nucleosomal glucocorticoid response element modulates glucocorticoid receptor affinity. *Genes Dev.*, **7**, 2471–2482.
34. Fields,A.P., Meyer,E.A. and Cohen,A.E. (2013) Euler buckling and nonlinear kinking of double-stranded DNA. *Nucleic Acids Res.*, **41**, 9881–9890.
35. Du,Q., Kotlyar,A. and Vologodskii,A. (2008) Kinking the double helix by bending deformation. *Nucleic Acids Res.*, **36**, 1120–1128.
36. Lionberger,T.A., Demurtas,D., Witz,G., Dorier,J., Lillian,T., Meyhofer,E. and Stasiak,A. (2011) Cooperative kinking at distant sites in mechanically stressed DNA. *Nucleic Acids Res.*, **39**, 9820–9832.
37. Demurtas,D., Amzallag,A., Rawdon,E.J., Maddocks,J.H., Dubochet,J. and Stasiak,A. (2009) Bending modes of DNA directly addressed by cryo-electron microscopy of DNA minicircles. *Nucleic Acids Res.*, **37**, 2882–2893.
38. Johnson,S., Chen,Y.J. and Phillips,R. (2013) Poly(dA:dT)-rich DNAs are highly flexible in the context of DNA looping. *PLoS One*, **8**, e75799.
39. Vafabakhsh,R. and Ha,T. (2012) Extreme bendability of DNA less than 100 base pairs long revealed by single-molecule cyclization. *Science*, **337**, 1097–1101.
40. Yuan,G.C., Liu,Y.J., Dion,M.F., Slack,M.D., Wu,L.F., Altschuler,S.J. and Rando,O.J. (2005) Genome-scale identification of nucleosome positions in S. cerevisiae. *Science*, **309**, 626–630.
41. Segal,E. and Widom,J. (2009) Poly(dA:dT) tracts: major determinants of nucleosome organization. *Curr. Opin. Struct. Biol.*, **19**, 65–71.